Supporting Information

S1 Supporting Figure S1

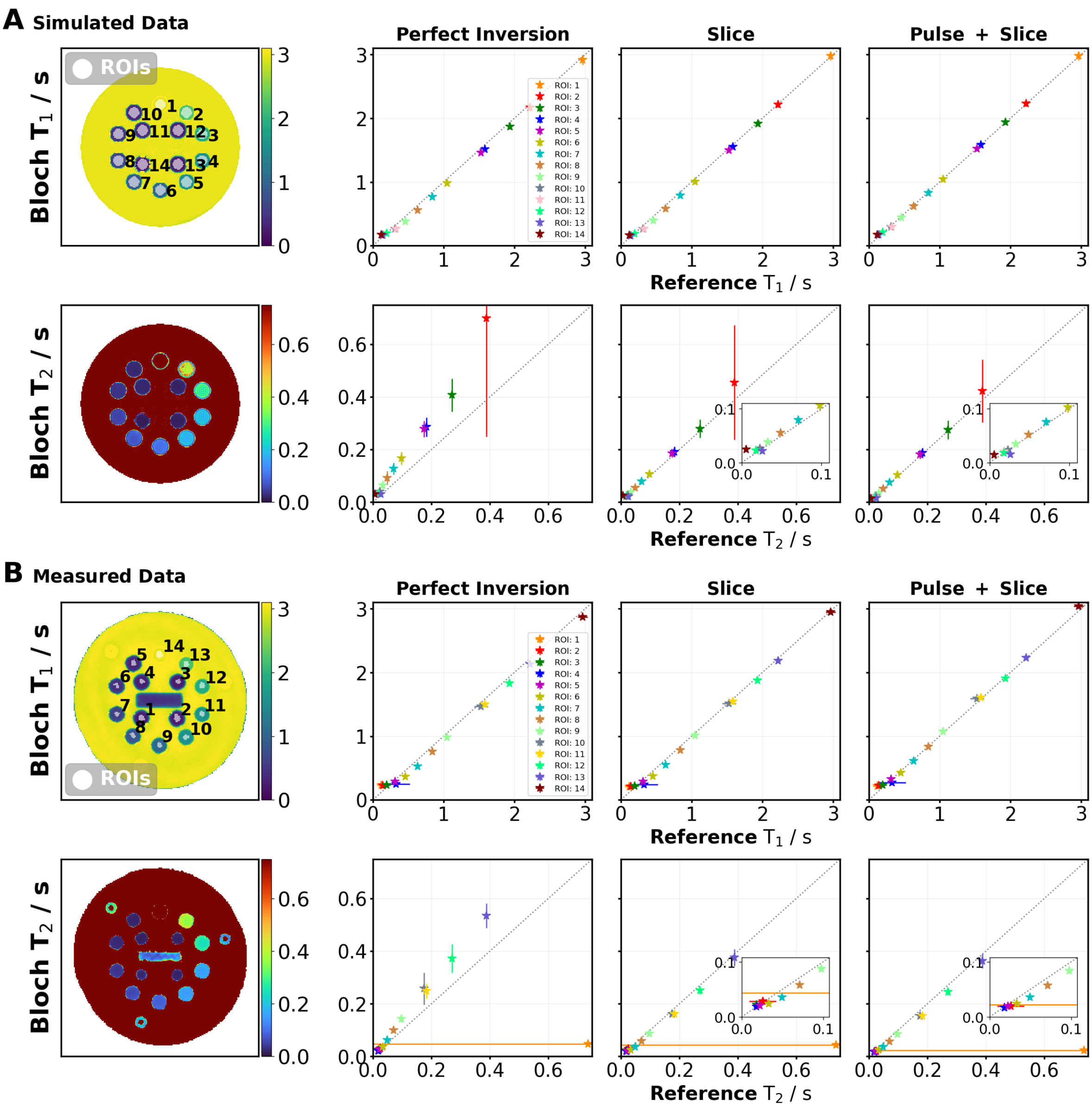

Figure S1: **A**: Reconstructed T_1 and T_2 parameter maps and the corresponding ROI values for numerical radial single-shot IR bSSFP data of a digital multi-coil reference object simulated in k-space. The left side shows the reconstructed parameter maps and the right the ROI analysis results relative to the simulated reference values with standard deviations. The analyzed ROIs are marked and numbered in the T_1 map. **B**: Reconstructed T_1 and T_2 parameter maps with corresponding ROI values for a radial single-shot IR bSSFP measurement of the T_2 spheres of the NIST phantom. The left side corresponds to the rightmost ROI analysis. The right side presents the comparison of the analyzed ROIs reconstructed with the Bloch model-based technique for various signal model assumptions. It is compared to gold-standard reference values.

S2 Supporting Figure S2

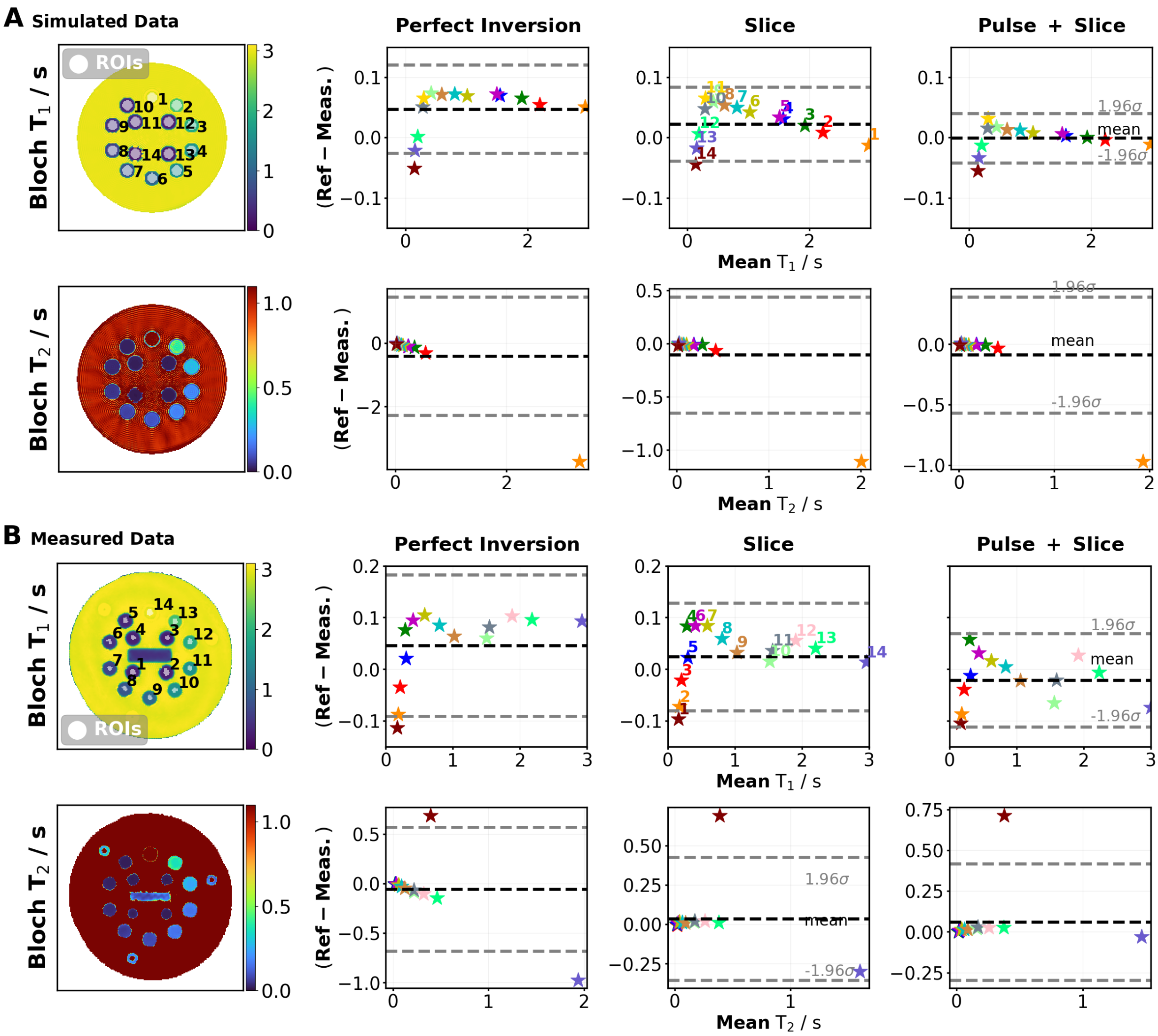

Figure S2: **A**: Reconstructed T_1 and T_2 parameter maps and all corresponding ROI values for simulated radial single-shot IR bSSFP data. Here, the data points removed to improve the visualization in Figure 5 are included. Reconstructed parameter maps are shown on the left. Bland-Altman plots comparing to the simulated reference values are added on the right. The ROIs are marked and numbered in the T_1 map. **B**: Reconstructed T_1 and T_2 parameter maps and the corresponding ROI values for a radial single-shot IR bSSFP measurement of the T_2 spheres of the NIST phantom. The left side corresponds to the rightmost ROI analysis. The right shows the Bland-Altman plots comparing the values of the ROIs reconstructed with the Bloch model-based technique for various assumptions used in the signal model compared with gold-standard reference values.

S3 Supporting Figure S3: Simulation Accuracy

This section discusses the simulation accuracy of the ODE solvers for different tolerances and sampling rates in more detail. In Figure S3.A reconstructions of the IR FLASH phantom from Figure 4.B using the Bloch model-based reconstruction with signal model assumptions of only on-resonant spins and with spins distributed along a slice-selection gradient are shown. The reconstructions are performed with varying tolerances for the STM simulation method while keeping the initial step-size of the RK54 solver constant at 1E-4.

For the on-resonance results the difference values are small. Here, the reconstructed parameter maps for higher error tolerances are very similar to the reference map. For the signal model with simulation of the slice-selection gradient the reconstructed parameter maps are similar up to a tolerance of 0.001, while lower values result in large variations in the T_1 parameter map. The important result is that the error of the simulation from an STM tolerance value of 0.001 still allows accurate reconstructions even for complex spin dynamics.

In Figure S3.B the error plot from Figure 3 is extended to include more simulations with different tolerances and sampling rates. The required STM tolerance of 0.001 from Figure S3.A for complex dynamics is translated to the required sampling rate for the ROT simulation. It shows the point-wise errors (PWE) for RK54, STM and ROT for the same simulation with slice-selection gradient. The tolerance value for the estimated limit of STM of 0.001 produces an error similar to the 1 MHz sampling rate. This leads to the conclusion that at least a sampling rate of 1 MHz is required for an accurate reconstruction of complex spin dynamics involving slice-selection gradients.

The simulation times for the same analysis with a slice-selection gradient, as presented in Figure 3, are shown in Figure S3.C for multiple tolerances and sampling rates.

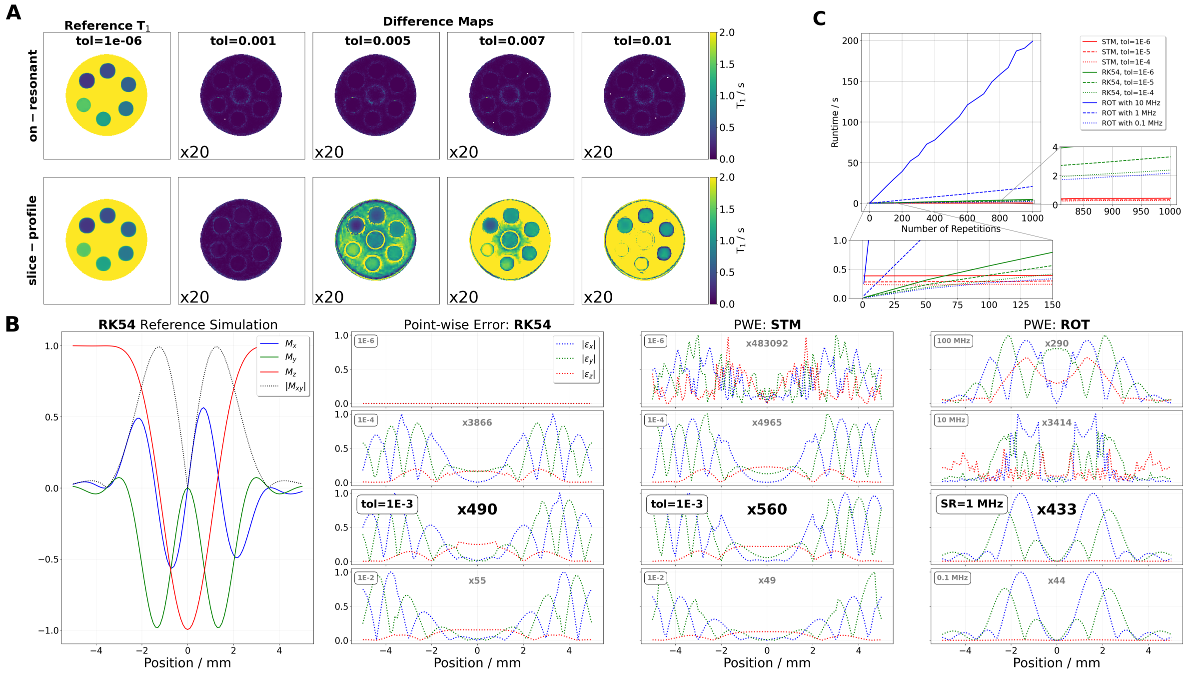

Figure S3: **A**: T_1 maps reconstructed from single-shot IR FLASH (same as for Figure 4.B) with varying tolerances of the STM simulation. The forward model assumes on-resonant spins. The differences of the reconstructions for tolerances of 1e-5 to 1e-2 compared to the 1e-6 reference are shown in the bottom row. The differences are scaled by large factors for improved visualization. **B**: Extension of Figure 3.A with varying tolerances for RK54 and STM and sampling rates for ROT. **C**: Extension of Figure 3.B with varying tolerances for RK54 and STM and sampling rates for ROT.

S4 Supporting Figure S4

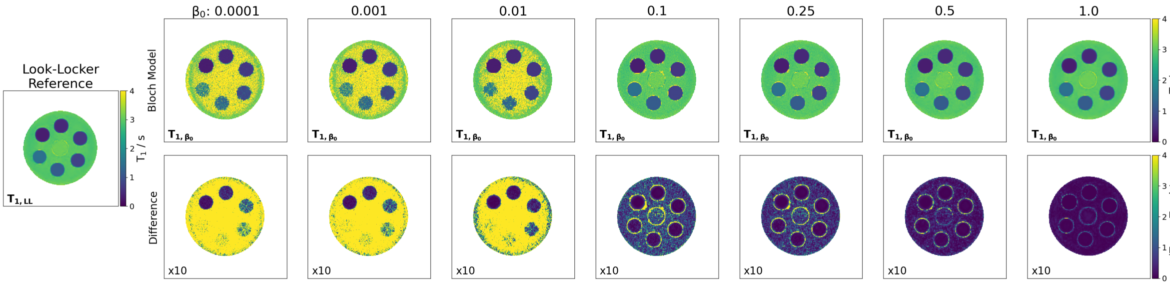

Figure S4: Reconstructed T_1 parameter maps similar to Figure 4.B for varying wavelet regularization strength β_0 for the Bloch model-based reconstruction (upper row). On the left a reference reconstruction estimated with the reparameterized Look-Locker model-based technique is shown. In the bottom row the differences between Bloch model-based reconstruction and the reference map are shown scaled by a factor of 10 for improved visualization.

S5 Supporting Figure S5: Influence of the Magnetization Transfer Effect

To estimate the influence of the magnetization transfer effect (MT) on the reconstructed T_1 parameter maps multiple single-shot IR bSSFP experiments were performed with varying TR and T_{RF}. The sequence parameters are shown in Table S2. The analytical representation of the signal behavior during an IR bSSFP experiment can be described by Equation (F1). Following [1] the MT effect reduces the T_1^* and the steady-state magnetization M_{ss}, while not affecting M_0. They propose an exponential model for correction of the effect of MT on M_{ss}:

$$M_{ss}(\beta) = \left(M_{ss}^{\text{no MT}} - M_{ss}^{\text{full MT}}\right) \cdot \left(1 - e^{-k \cdot \beta}\right) + M_{ss}^{\text{full MT}} \tag{1}$$

Here, the signal which is not affected by MT is denoted as $M_{ss}^{\text{no MT}}$, the signal from a fully-saturated solid pool is $M_{ss}^{\text{full MT}}$, the rate constant is k and the increase in RF pulse duration is β.

The T_1 value for an IR bSSFP can be estimated by

$$T_1 = \frac{T_1^*}{M_{ss}} M_0 \cos\left(\frac{\alpha}{2}\right) \tag{2}$$

with the flip angle α.

Taking into account that T_1^* is less affected by MT than M_{ss} [1], we assume that the MT influence on T_1 follows the model:

$$T_1(\beta) \approx \frac{1}{(a-b) \cdot (1 - e^{-k' \cdot \beta}) + b} \ . \tag{3}$$

Equation 3 is fitted to the different relaxation parameters from various acquisitions with different TR and T_{RF} (Figure S5).

The estimated parameters a, b and k' have no direct physical interpretation, but can be used to interpolate an MT-free T_1 for $\beta \to \infty$. The parameters of the fits are shown in Table S1.

The results for $T_1(\beta \to \infty)$ suggest that the MT effect plays a significant role in the T_1 offset observed in Figure 6 , but also indicates that it might not explain the complete discrepancy.

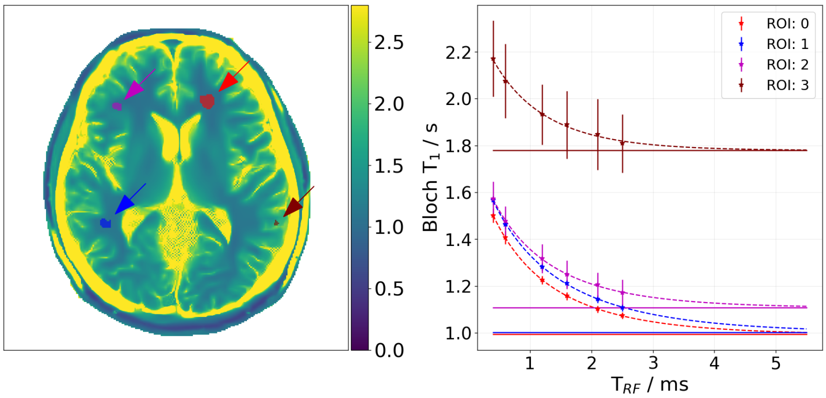

Figure S5: Visualization of the magnetization transfer effect in T_1 maps reconstructed from an IR bSSFP sequence with varying TR and T_{RF}. On the left the T_1 map corresponding to the longest $T_{RF} = 2.5$ ms is plotted with colored ROIs. The mean values of the relaxation values for the colored areas are plotted with their standard deviation on the right for various lengths of RF pulses T_{RF}. The dotted lines represent the fitted functions following the analysis of Section S5.

S6 Supporting Figure S6

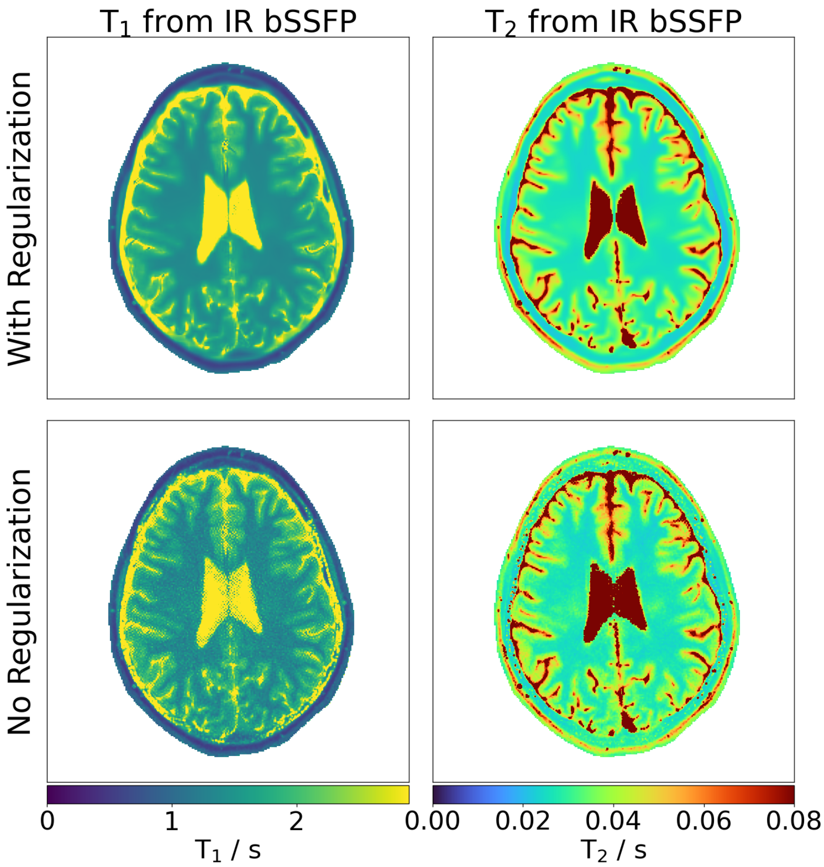

Figure S6: Bloch model-based reconstruction of an in vivo single-shot IR bSSFP dataset acquired with 1 ms long RF pulses. The coil-sensitivities have been estimated with the regular Bloch model-based method and have been added as fixed prior knowledge to both reconstructions afterwards. The top presents the regularized reconstruction, while the bottom results do not include any regularization on the parameter maps.

S7 Supporting Table S1

Table S1: Table listing the fitting parameters estimated for Figure S5.

	a [s]	b [s]	k' [s]
ROI 1	0.931±0.006	0.510±0.003	0.723±0.023
ROI 2	0.923±0.013	0.498±0.005	0.620±0.041
ROI 3	0.834±0.01	0.498±0.006	0.786±0.059
ROI 4	0.519±0.007	0.382±0.008	0.992±0.158

S8 Supporting Table S2

Table S2: Table listing the sequence parameters for the analysis in Figure S5.

Sequence	IR bSSFP	IR bSSFP	IR bSSFP	IR bSSFP	IR bSSFP	IR bSSFP
Object	in vivo	in vivo	in vivo	in vivo	in vivo	in vivo
TR|TE [ms]	3.8|1.9	4.0|2.0	4.6|2.3	5|2.5	5.5|2.75	6.14|3.07
FA [°]	35	35	35	35	35	35
T_{RF} [ms]	0.4	0.6	1.2	1.6	2.1	2.5
Nominal Slice Thickness [mm]	5	5	5	5	5	5
Repetitions	1000	1000	1000	1000	1000	1000
Coils	20	20	20	20	20	20
BWTP	1	1	1	1	1	1
BR	256	256	256	256	256	256
FoV [mm]	200	200	200	200	200	200
Duration [min:s]	0:04	0.04	0:05	0:05	0:06	0:06
others	#tiny GA=13	#tiny GA=13	#tiny GA=13	#tiny GA=13	#tiny GA=14	#tiny GA=13

References

[1] Ehses Philipp, Seiberlich Nicole, Ma Dan, et al. IR TrueFISP with a golden-ratio-based radial readout: Fast quantification of T1, T2, and proton density. *Magn. Reson. Med.*. 2013;69(1):71-81.